Applied Nanoscience (2020) 10:379–389
https://doi.org/10.1007/s13204-019-01185-0

ORIGINAL ARTICLE

Central composite design-based optimization and fabrication of benzylisothiocynate-loaded PLGA nanoparticles for enhanced antimicrobial attributes

Ankush Parmar[1] · Gurpreet Kaur[1] · Shikha Kapil[2] · Vipasha Sharma[2] · Shweta Sharma[1]

Received: 12 February 2019 / Accepted: 5 October 2019 / Published online: 23 October 2019

Abstract
Benzylisothiocynate also referred to as BITC is a compound which is commonly found in Cruciferae plants. This chemical moiety falls under the category of Isothiocynates (ITCs), and is known to possess superior antibacterial properties. Hence, endeavors have been made in the present research to encapsulate benzyl isothiocynate (BITC) within the framework of polymeric nanoparticles to enhance its potency, stability, safety, and biocompatibility. The study also aimed at fabricating a nanoparticulate system with engineered release characteristics so that the susceptibility of BITC in evoking a bactericidal response towards *E. coli* can be enhanced. To attain an optimal system with desired critical quality attributes [CQAs (particle size, entrapment efficiency and release)] all the requisite critical material attributes [CMAs (amount of polymer, and concentration of surfactant)] were optimized using central composite design (CCD). An overall assessment of the physicochemical characteristics of fabricated PLGA nanoparticles containing BITC viz. BITC-PLGA NPs were accomplished using DLS, FE-SEM, UV–Vis, and ATR-FTIR spectroscopy. The BITC-PLGA NPs were found to be 106.2 ± 1.78 nm in size, and has a surface charge of − 16.3 ± 0.64 mV. The BITC-PLGA NPs were found to be homogenous as the DLS analysis revealed a PDI value of 0.353 ± 0.008. A significantly high entrapment efficiency and percentage loading (~ 74 and 32%) along with a sustained release of BITC (~ 64.2 (pH 5.5)–(pH 5.5), and 83.8 (pH 7.4) %) was obtained from BITC-PLGA NPs. The antibacterial assay also pointed towards a safe and efficient delivery system which can further prove to be a pioneer in the upcoming times.

Keywords Central composite design · Benzyl isothiocynate · PLGA · Antibacterial · Nanoparticles

Introduction

Since time immemorial, the organosulfur compounds, Isothiocyanates (ITC_s) have gained momentous zeal and enthusiasm. They have been considered to be of prime significance owing to their medicinal properties. Ancient literature depicts several instances, where herbs comprising of ITC_s were predominantly used as preservatives, cleaning agents, spices, and antimicrobial agents (Sofrata et al. 2011). Plants and vegetables belonging to Cruciferae family are the major sources from where ITC_s can be obtained naturally in abundance (Encinas-Basurto et al. 2017; Khoobchandani et al. 2012). Amidst all ITC_s family, Benzyl Isothiocyanate also commonly referred to as BITC is one of the most commonly occurring phytoconstituent (Encinas-Basurto et al. 2017). BITC is known to possess several alluring properties such as enhanced bactericidal and apoptotic activity, catalyzes ROS activity thereby inhibiting NFkβ activity, cell cycle arrest which allows it to bag top position amongst the category of vital bioactive (Hecht 1999; Prashar et al. 2012). Apart from these, BITC have been found to possess sensitivity towards varied microbial agents and are capable of inducing an anti-helminthic and vermifungal activity at infinitesimally low concentrations (Dufour et al. 2015). In context to this,

Electronic supplementary material The online version of this article (https://doi.org/10.1007/s13204-019-01185-0) contains supplementary material, which is available to authorized users.

✉ Shweta Sharma
25shweta@pu.ac.in

[1] Institute of Forensic Science and Criminology, Panjab University, Chandigarh 160014, India

[2] University Institute of Biotechnology, Chandigarh University, Gharuan, Chandigarh, Punjab 140413, India

a study conducted by Li et al. (2015) demonstrated that the phytoconstituents of cruciferous vegetables were potent enough to incite an enhanced antimicrobial response in comparison to the traditional antibiotics. Hence, it became imperative on the basis of these facts, and findings that BITC can act as a safe, and efficient alternative to combat the overgrowing menace of microbial-based infractions (Dufour et al. 2015).

Despite these alluring properties, hydrophobicity, diminished bioavailability, degradation, and pungent odor are some of the grave factors which tend to hamper the practical utility of these diverse molecules in the domain of biomedical sciences. Other factors such as volatility, and strong electrophilic nature make it more susceptible towards nucleophilic attacks by active molecules bearing functional groups like SH, NH_2, H_2O, and OH (Desai and Park 2005; Hanschen et al. 2012; Liu and Yang 2010). This further worsens the situation as it becomes difficult for scientists and researchers to select the appropriate dose regimen for an enhanced therapeutic efficacy. Another point of concern is the rapid metabolism of this active constituent into *N*-acetyl-*S*-(*N*-benzylthiocarbamoyl)-L-cysteine owing to which approximately 53% of BITC is straightaway eliminated out of the body (Mennicke et al. 1988). Several studies have also shown that in vivo distribution of BITC results in the formation of protein and enzyme conjugates which ultimately diminishes its therapeutic potential (Jang et al. 2013; Rozhkova et al. 2009).

To overcome the above-mentioned lacunas researchers and scientists all across the globe are making continuous efforts to pave a unanimous one pit solution. In context to this, pertinent reports are available in the literature where varied carriers have been designed for improvising the solubility, bioavailability, tailored release characteristics, residence time and bactericidal properties of BITC (Bohrey et al. 2016; Jiang et al. 2006; Li et al. 2019; Ohta et al. 2004a, b; Qhattal et al. 2011; Yuan et al. 2009). Whilst, burst release, non-uniform sized particles and irregular geometries are some of the unavoidable constraints which left these systems with an iota of doubt and restricted their implementation on a broader perspective.

Meanwhile, it became apparent from several studies that facile encapsulation of BITC in the matrix of polymeric nanoparticles offers several advantages such as (Bhujbal et al. 2014; Fathi et al. 2012; Fernandes and Gracias 2012; Gaurav et al. 2018);

(i) Enhanced stability towards harsh physiological milieu.
(ii) Tailored release characteristics.
(iii) Sustained release of active moiety at designated target site.

Poly-D, L-lactide-co-glycolide (PLGA) is a FDA-approved biodegradable polymer which has become globally renowned for its application in the field of biomedical sciences (Sharma et al. 2016). Its tremendous physicochemical properties have made it an ideal vector for drug delivery applications (Armentano et al. 2010; Danhier et al. 2012; Lü et al. 2009; Sharma et al. 2018). However, till date, the copolymer has been never utilized for the delivery of BITC. Hence, the present research emphasizes on making an incessant attempt to comprehensively circumvent the existing hurdles by fabricating BITC-loaded PLGA nanoparticles (BITC-PLGA NPs). The present examination consequently also aims at efficiently assessing every essential process and formulation parameter in terms of their effect on the key quality attributes, i.e. particle size, zeta potential and drug release (%) utilizing a combinational central composite design (CCD)-based approach to diminish the quantity of investigations and to build models of predictions. State of art analytical technique-based investigation was also carried out to exfoliate the intrinsic properties of the BITC-PLGA NPs. In vitro release studies (IVRs) were conducted to assess the drug release characteristics of the formulated NPs. Haemocompatibilty studies were conducted to evaluate the safety of the formulation. Additionally, antibacterial studies were conducted to explore the real time biological potential of the BITC-PLGA NPs.

Materials and methods

Materials

PLGA (50:50), BITC (98%, FG), and acetone were procured from Sigma-Aldrich Pvt. Ltd. (India). Vitamin E TPGS was a generous gift from Isochem (Vert Le Petit, France). Dialysis membrane tubing was purchased from HIMEDIA (Mumbai, India)

Fabrication of BITC-loaded PLGA nanoparticles (BITC-PLGA NPs)

BITC-PLGA NPs were prepared via quasi-emulsification solvent diffusion technique as reported elsewhere with suitable modifications (Encinas-Basurto et al. 2017; Ibarra et al. 2015). BITC, and PLGA were appropriately weighed, and a suitable quantity was taken for further experimentation. Previously weighed samples were dissolved in acetone to obtain an organic phase. Post preparation the organic phase was subsequently added to an aqueous emulsifier/surfactant phase comprising chiefly of TPGS in a drop wise manner. To ensure a thorough homogenization

and solvent evaporation the organic-aqueous phase/oil–water emulsion was stirred on a magnetic stirrer for about 6 h. The preformed emulsion was later centrifuged to segregate even-sized nanoparticles, and repeatedly given water washings to remove other unwanted excipients. The purified BITC-PLGA NPs were lyophilized, and kept in a desiccator until further experimentation.

Characterization of BITC-PLGA NPs

Physicochemical characterization

Morphology A thorough investigation of the surface morphology and geometrical attributes was accomplished on Hitachi SU 8010 field emission scanning electron microscope (FE-SEM). A drop of BITC-PLGA NPs was placed on a copper grid and it was allowed to get air dried. Post drying, sputtering of the sample was done using MC 1000 sputter coater and the grid was then finally analyzed at an operating voltage of 5 kV.

Particle size and polydispersity index (PDI) Hydrodynamic diameter and PDI of the BITC-PLGA NPs were determined by dynamic light scattering (DLS) measurements. For this a suitably diluted aliquot (1 mL) of BITC-PLGA NPs was analyzed using Beckman Coulter, Delsa™ Nano series (CA, USA) zeta sizer. Nanoparticle size was determined using a Zetasizer employing a nominal 5-mW He–Ne laser operating at 633 nm wavelength. The scattered light was detected a 135° angle. The refractive index (1.33) and the viscosity (0.89) of ultrapure water at 25 °C were used for size measurements. The measured nanoparticle sizes were presented as the average value of 20 runs, and experiments were done in triplicate. The polydispersity index of the particle size was measured using the same instrument on a scale from 0 to 1.

Zeta potential Zeta potential was determined on the basis of electrophoretic mobility under an electric field using a zeta sizer [Nano-Zetasizer ZS, Malvern Instrument Ltd. (UK)]. To measure the zeta potential, a dilute suspension of the NPs was prepared by re-suspending 0.1 mg of lyophilized NPs in 1 mL of distilled water at pH 7.4. To create a homogeneous suspension, the particles were sonicated in a bath sonicator for 30 s and the zeta potential was measured in triplicate.

FTIR spectroscopy ATR-FTIR spectra were recorded using Spectrum Two' FTIR spectrophotometer (Perkin Elmer) within a spectral range of 4000–400 cm^{-1}. Absorption spectra were recorded using Shimadzu 2550 PC series UV–Vis spectrophotometer.

Encapsulation efficiency and loading

A quantitative estimation of the amount of active biomolecule entrapped in the fabricated BITC-PLGA NPs was conducted via employing an indirect method (Gonzalez-Pizarro et al. 2018). The BITC-PLGA NPs were centrifuged at 15,000 rpm for 10 min and the free drug (suspension) was collected. Aliquots of the collected suspension were taken and appropriated dilutions were performed. Post dilution, the sample was imposed to undergo UV–Vis spectrophotometric analysis and the entrapment efficiency (% EE) was calculated according to the following equation:

$$\%\,\mathrm{EE} = \frac{\text{Amount of BITC feed} - \text{Amount of BITC in supernatant}}{\text{Amount of BITC feed}} \times 100. \quad (1)$$

Subsequently, percentage loading (% L) capacity of the BITC-PLGA NPs was also calculated using the following equation:

$$\%\,\mathrm{L} = \frac{\text{Total amount of BITC} - \text{Amount of free BITC}}{\text{Weight of BITC-PLGA-NPs}} \times 100. \quad (2)$$

In vitro drug release

The release of test specimen (BITC-PLGA NPs) was performed in pH progression medium simulating the physicochemical milieu. Dialysis bag methodology was utilized for assessing the in vitro drug release of the active constituent from the test formulations. BITC-PLGA NPs (2 mL) was sealed in a dialysis bag membrane and stirred in PBS. The release studies were accomplished in both acidic (5.5) and basic (7.4) pH. Throughout the experimentation, the stirring rate and temperature were maintained at 100 rpm and 37 °C. At requisite time interval, appropriate amount of samples (3 mL) was withdrawn. The dissolution media were replenished after subsequent withdrawal to maintain perfect sink conditions. The quantitative determination of BITC was accomplished via analyzing the withdrawal samples using UV–Vis spectrophotometric analysis. The results obtained after in vitro studies were further screened using varied mathematical models and the appropriate kinetic model depicting the best fit was chosen. The kinetic modeling of release data was performed using Kinet DS software (Mendyk and Jachowicz 2007).

Stability study

The long-term stability studies were adopted as per the ICH guidelines to intrigue the intrinsic stability of the developed BITC-PLGA NPs. The fabricated PLGA NPs were stored for 30 days at a temperature of 4 °C. Periodic assessment was performed by DLS to assess any change in the average particle size, and zeta potential of the aforesaid formulation.

Haemocompatibilty studies

First, whole blood was collected from healthy volunteers and it was placed in heparinized centrifuge tubes. Post collection, the sample was centrifuged (2500 rpm × 10 min) and the plasma was removed. Subsequent washings with PBS were given to remove an engulfed material. Lately, the haematocrit cell suspension (1.5 mL) was appropriately mixed with 2.5 mL test (BITC-PLGA NPs) and control (BITC and PLGA NPs) samples. The samples were incubated at room temperature for pre-determined time interval. After 30 min the samples were centrifuged and corresponding absorbance was noted at 540 nm. Triton X-100 (1%) and PBS served as positive and negative controls, respectively. Percentage hemolysis (% H) was calculated according to the following equation:

$$\%\,\mathrm{H} = \frac{\text{Absorbance of sample} - \text{Absorbance of negative control}}{\text{Absorbance of positive control} - \text{Absorbance of negative control}}. \quad (3)$$

Antimicrobial studies

Agar well diffusion assay

Bactericidal potential of the fabricated system was explored using agar well diffusion assay (Balouiri et al. 2016; Francis et al. 2018). First, *E. coli* was cultured on Mueller–Hinton agar plates using spread plating technique. Subsequently, appropriate aliquots (150 µL, 100 µM) of test (BITC-PLGA NPs) and control [(Norfloxacin (NFC)), PLGA NPs, and BITC] samples were loaded into the wells punched in the agar plates. Post loading, the treated plate was incubated at an ambient temperature (37 °C/24 h) and the respective zone of inhibition was noted.

Time kill assay

Previously reported methodology of Zhou et al. and Chen et al. with slight modification was employed for assessing the antimicrobial activity of test (BITC-PLGA NPs) and control (BITC, NFC, and PLGA NPs) samples against *E. coli* (Shiguo et al. 2019; Wanjing et al. 2018). Herein, the quantitative estimation of antibacterial activity was accomplished using a viable cell count method. The protocol used was as follows: bacterial solution (10 mL, 10^5 CFUs/mL) and neutralizing broth (1 mL) were first added with the test samples (100 µL), and then they were covered. The treated samples were then subsequently incubated for a period of 24 h under controlled environmental conditions [temperature (37 ± 1 °C), and relative humidity (90%)]. Post incubation, the treated samples were thoroughly washed with 5 mL aqueous NaCl solution (0.85%, pH ~ 7.0), and the number of colonies formed was counted.

Results and discussion

Preparation and optimization of BITC-PLGA NPs

The quasi-emulsification solvent diffusion technique used in the present study successfully leads to the fabrication of stable PLGA nanoparticles (Encinas-Basurto et al. 2017). To fabricate a model drug delivery system possessing all the requisite characteristics, experimental design-based systematic optimization of BITC-PLGA NPs was carried out (Dewangan et al. 2018). The requisite critical material attributes (CMAs) which tend to have an intricate effect on critical quality attributes (CQAs) were chosen (Table S1.). The selected CQAs were subsequently screened using two-factor five-level central composite design (CCD) and optimal values of these variables were attained (Table S2.). Design expert software (Version 11, Trial, Stat-Ease Inc. Minneapolis, USA) was used for obtaining the data. The obtained data were further imposed to undergo statistical analysis using ANOVA and second-order polynomial equation was used to model the responses. The polynomial equation was framed by taking into consideration the statistically significant coefficients ($P > 0.05$). Post statistical analysis multiple linear regression analysis (MLRA) was performed, and varied coefficients such as regression coefficients and multiple correlation coefficient (R^2 and adjusted R^2) were calculated (Table S3). For understanding the relationship among the considered CMAs on CQAs, response surface mapping was completed utilizing 3D-resposne surface plots, and 2D-contour plots (Beg et al. 2018). To select the optimal batches desirability function-based approach was employed (Dewangan et al. 2018). Whilst a due care was taken to attain a maximum entrapment efficiency, drug release along with a minimum particle size.

Particle size

The outcome of the present study clearly indicated that the fabricated nanoparticles possessed smaller particle size (Y_1) values ranging between 86.43 and 242.91 nm (Table S4). Statistical analysis of the quadratic model for particle size revealed a model P and F value of < 0.0001 and 71.84, respectively. It can be comprehensively said on the basis of these model values that the design model is highly significant. The total variability in the model can be explained on the basis of coefficient of determination (R^2) (Saka et al. 2018). The R^2 was found to be 0.9809 which indicates that the designed model is capable of explaining the ~ 98% variation in the studied response. However, the remaining 2% variation can be attributed to the noise.

Suitability of the present quadratic model is also proved owing to the presence of higher value of R^2 as compared to the adjusted R^2 (0.9672). The predicted R^2 of 0.8609 is in reasonable agreement with the adjusted R^2 as the difference among themselves is less than 0.2 which further strengthens the above mentioned findings. Another statistical parameter which plays a pivotal role in explaining the signal to the noise ratio is the Adeq. Precision. As the observed value for Adeq. Precision (~ 20.87) was found to be greater than four hence it can be righteously said that the model can be used to navigate the design space. The correlation between the chosen CMAs and CQAs was established as per the polynomial equation (Eq. 4):

$$Y_1 = 111.53 + 16.93 \times A + 9.51 \times B - 16.38 \times AB + 103.13 \times A^2 - 10.99 \times B^2. \quad (4)$$

For providing an improvised product and process understanding, 3D surface and 2D contour plots tends to establish an intricate cause and effect relationship amongst the examined factors. The response surface investigation uncovered noteworthy impact of CMAs, on all the chosen CQAs. Figure S1. (a) portrays an inverted stationary ridge type 3D-response surface plot for particle size. The figure clearly points that an inverse relationship existed among the release and surfactant's concentration. It became quite apparent from the figure that a declination in the amount and concentration of both the polymer and surfactant leads to a decrease in particle size. Whilst, a vice-a-versa phenomenon was observed when the value of both the CMAs was escalated. Further, at intermediate levels of both the excipients, median size particles were formed. Besides, 2D-contour plot delineated in Figure S1. (b) Similarly depicted analogous observation with existence of interaction effect, which can be clearly visualized from the curved contour lines (Beg et al. 2018).

Entrapment efficiency (%)

The outcome of the present study clearly indicated that the fabricated nanoparticles possessed higher entrapment efficiency (Y_2) values ranging between 57.82 and 74.98 nm (S. Table 4). Statistical analysis of the quadratic model for particle size revealed a model P and F value of < 0.0001 and 102.69, respectively. It became apparent from the outcome of the statistical analysis that the selected model design is highly significant. Further, to decipher the total variability in the selected model design coefficient of variation (R^2) was assessed (Saka et al. 2018). The R^2 was found to be 0.9866 which indicates that the designed model is capable of explaining the ~ 98% variation in the studied response. However, the remaining 2% variation can be attributed to the noise.

Suitability of the present quadratic model is also proved owing to the presence of higher value of R^2 as compared to the adjusted R^2 (0.9769). The predicted R^2 of 0.8698 is in reasonable agreement with the adjusted R^2 as the difference among themselves is less than 0.2 which further strengthens the above-mentioned findings. Another statistical parameter which plays a pivotal role in explaining the signal to noise ratio is the Adeq. Precision. As the observed value for Adeq. Precision (~ 28.88) was found to be greater than 4 hence it can be righteously said that the model can be used to navigate the design space. The correlation between the chosen CMAs and CQAs was established as per the polynomial equation (Eq. 5):

$$Y_1 = 74.54 - 0.5850 \times A - 3.28 \times B - 1.40 \times AB - 3.77 \times A^2 - 6.94 \times B^2. \quad (5)$$

3D-response surface design plot for entrapment efficiency is portrayed in Figure S2. (a) (Beg et al. 2018). A curvilinear shape response surface plot depicting a non-linear trend was obtained. It was observed that, an inverse relationship existed among the entrapment efficiency and surfactant's concentration. Here, a diminished entrapment was obtained with an increase in the concentration of surfactant. Whilst, a vice-a-versa trend was followed in case of amount of polymer where a gradual increase in the entrapment efficiency was observed with increasing amount of polymer. However, at intermediate levels of both the excipients, maximum extraction of BITC was achieved. In addition, 2D-contour

plot delineated in Figure S2 (b) similarly depicted analogous observation, which can be clearly visualized from the curved contour lines (Beg et al. 2018).

Drug release (%)

The outcome of the present study clearly indicated that the fabricated nanoparticles possessed a sustained release (Y_2) values ranging between 12.59 and 58.63 nm (S. Table 4). Statistical analysis of the quadratic model for particle size revealed a model P and F-value of < 0.0001 and 259.21, respectively. It became imperative from these findings that the proposed design is vastly significant. Coefficient of variation (R^2) was further determined to assess the total variability existing in the optimization model (Saka et al. 2018). The R^2 was found to be 0.9946 which indicates that the designed model is capable of explaining the ~ 99% variation in the studied response. However, the remaining 1% variation can be attributed to the noise.

Suitability of the present quadratic model is also proved owing to the presence of higher value of R^2 as compared to the adjusted R^2 (0.9908). The predicted R^2 of 0.9642 is in reasonable agreement with the adjusted R^2 as the difference among themselves is less than 0.2 which further strengthens the above mentioned findings. Another statistical parameter which plays a pivotal role in explaining the signal to the noise ratio is the Adeq. Precision. As the observed value for Adeq. Precision (~ 53.13) was found to be greater than four hence it can be righteously said that the model can be used to navigate the design space. The correlation between the chosen CMAs and CQAs was established as per the polynomial equation (Eq. 6);

$$Y_1 = 74.54 - 0.5850 \times A - 3.28 \times B - 1.40 \times AB - 3.77 \times A^2 - 6.94 \times B^2 \quad (6)$$

3D-response surface design plot for release (%) is portrayed in Figure S3 (a) (Beg et al. 2018). An inverted stationary ridge type response surface plot depicting a non-linear trend was obtained. It was observed that, an inverse relationship existed among the release and surfactant's concentration. It became quite apparent from the figure that, a declination in the amount and concentration of both the polymer and surfactant lead to a decrease in release (%) of BITC. Whilst, a vice-a-versa phenomenon was observed when the value of both the CMAs were escalated. Further, at intermediate levels of both the excipients, a comparatively sustained release of active constituent was observed. Besides, 2D-contour plot delineated in Figure S3 (b) similarly depicted analogous observation with existence of interaction effect, which can be clearly visualized from the curved contour lines (Beg et al. 2018).

Model diagnostic plots

The fitness of the considered model for individual CQAs was deciphered via employing model diagnostic plots (Beg et al. 2018). The obtained normal plots demonstrated a collinear trend for the individual consolidated attributes. It was observed that the data points were scattered around the best fit line (Figure S4). The following demarcating observations were further strengthened by the predicted vs. actual (Figure S5) and residual vs. run plots (Figure S6), respectively. Similar patterns for all the individual CQAs were obtained in both the plots and it was noted that the data points were randomly scattered alongside the base line in case of both the aforementioned plots.

Whilst, in case of residual vs. run plots the data points were found to be situated in a crisscross pattern around the residual line. Further, similar observations were attained in case of leverage (Figure S7) where it was noticed that the data points were distributed in a randomly ordered fashion with the absence of outliers. Box-Cox plots portrayed in Figure S8 additionally depicts the presence of green line delineating the data within 95% confidence interval and do not require any power transformation for the purpose (Beg et al. 2018).On the premises of these facts that it can be said that the proposed CCD model clearly depicted linearity, sensitivity and specificity.

Search for the optimal formulation

A combinatorial approach employing numerical and graphical optimization methodology was employed for searching the optimal formulation. Here, the objectives were set for the CQAs to attain the desirable characteristics, i.e. smaller particle size, sustained release, and maximum entrapment efficiency (Beg et al. 2018). In lieu of the detailed numerical evaluation, the formulation relating to the coded levels viz. amount of polymer (97.960) and concentration of surfactant (0.253) was found to be optimal. It might be attributed to the fact that the chosen formulation yielded a desirability value of ~ 1 (Figure S9). Further, graphical optimization was carried out within the analytical design space to narrow down the constraints for selecting an optimum formulation. Figure S10 depicts the overlay plot for optimized BITC-PLGA NPs in 2D design space. The obtained overlay design plot pointed that the developed CCD model is highly accurate.

Characterization of optimized BITC-PLGA NPs

Physicochemical characterization

A diverse array of systems has been designed for the facile encapsulation of BITC (Yuan et al. 2009). However, to

the best of our knowledge this is the first incessant attempt where PLGA-based nanoparticles have been employed for designing an anti-bacterial therapeutic vessel encompassing BITC (Encinas-Basurto et al. 2017). As revealed by DLS, the average particle size, zeta potential and PDI of the fabricated BITC-PLGA NPs was found to be 106.2 ± 1.78 nm, -16.3 ± 0.64 mV, and 0.353 ± 0.008, respectively (Figure S11 (a), (b)). The outcome of the DLS analysis portrayed that the fabricated particles are highly stabilized in nature and represents a uniform nano dimensional population. Figure S11(c) depicts the FE-SEM microphotograph of optimized BITC-PLGA NPs. The microphotograph correlated the results of DLS analysis, as the fabricated PLGA NPs were nano sized, mono-disperse, homogenous in nature and possessed a spherical geometry (Kunyi et al. 2018). The stable nature of the nanoparticles was also proven as no sign of aggregation was present. These facts vouched the appropriateness of fabricated BITC-PLGA NPs as potent vector for drug delivery with desired attributes.

Entrapment efficiency (% EE) and percentage loading (% *L*)

Formerly reported protocol of Dewangan et al. (2018) was employed for the quantitative assessment of entrapment efficiency and percentage loading of BITC-PLGA NPs. The % EE and % *L* were found to be and ~ 74 and 32%, respectively.

Spectroscopic analysis

UV–Vis The spectrophotometric analysis of BITC within a wavelength range of 200–800 nm yielded an absorption spectra having a λ_{max} of 254 nm which is characteristic for BITC (Fig. 1a). Whereas, on the other hand, the spectra of BITC-PLGA NPs did not show any peak in the character-

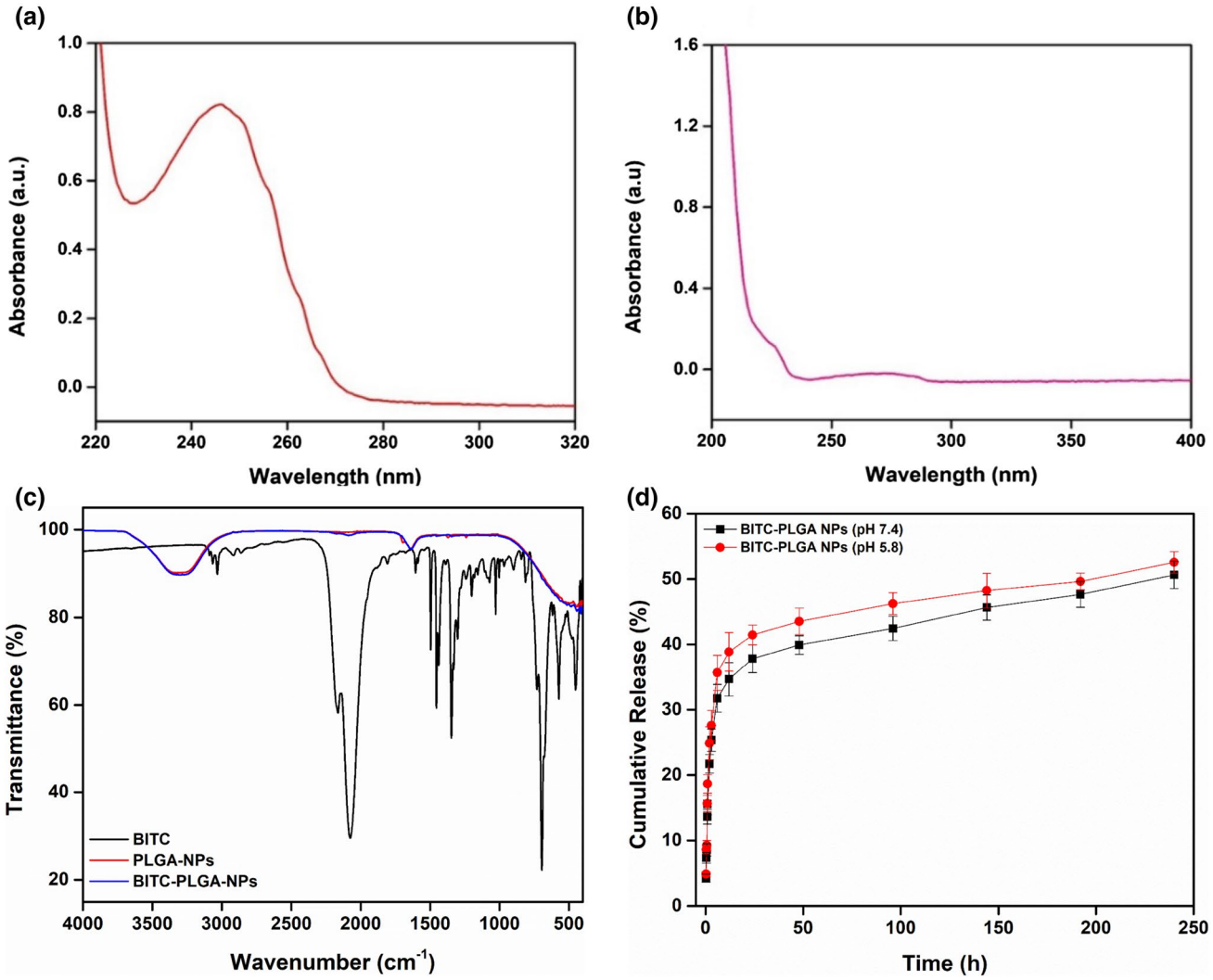

Fig. 1 UV–Vis spectra of **a** BITC and **b** BITC-PLGA NPs. **c** ATR-FTIR spectra of BITC, PLGA-NPs, and BITC-PLGA NPs. **d** Cumulative in vitro release of BITC from BITC-PLGA NPs

istic absorption region of BITC which further vouched the successful incorporation of active moiety into the PLGA nanoparticles (Fig. 1b).

ATR-FTIR Further, ATR-FTIR spectroscopy was performed to ascertain the integrity of the results obtained from UV–Vis analysis. Figure 1c demonstrates the FTIR spectra of BITC, PLGA NPs and BITC-PLGA NPs. It can be seen from the figure that the characteristic peak corresponding to the isosulfocyanic group (N=C=S) of BITC is missing in case of B PNPs. Hence on the premises of this it can be righteously said that the BITC was successfully encapsulated within the matrix of PLGA NPs (Yuan et al. 2009).

In vitro release and kinetic modeling study

BITC has been known to possess poor dissolution properties owing to its highly hydrophobic nature. However, a potent solution to this grave lacunae has been offered by the unique niche provided by the PLGA molecule. The facile encapsulation of BITC within the polymeric matrix results in the attainment of sustained release and desired dose regimen at the designated target site. Further, the PLGA molecule increases the retention time and diminishes any slight probability of evoking an unwanted potential side effect. Hence, to establish the controlled release profile of the fabricated BITC-PLGA NPs in vitro release studies were carried out in simulated physiological PBS buffer. The entire experimentation was carried out for a time interim of 6 h at acidic and neutral pH in controlled environmental conditions Fig. 1d.

A similar type of release profile was observed in case of both the buffer media, i.e. acidic (5.5) and basic (7.4) pH. It can be clearly visualized from the figure that initial phase of dissolution study followed a burst release pattern and 32.8 ± 0.69 (pH 5.5)–47.5 ± 0.76 (pH 7.4)% of BITC was released within 8 h of incubation. In the second phase, a steady release of active moiety took place where 53.7 ± 0.99 (pH 5.5)–74.6 ± 1.1 (pH 7.4)% of BITC was released post 72 h of incubation. Whereas, te latter phase (up to 168th h) followed a sustained release profile, and 64.2 ± 1.42 (pH 5.5)–83.8 ± 1.5 (pH 7.4)% of BITC was released in the dissolution media. Another, noteworthy point which came into consideration is the faster release of BITC from BITC-PLGA NPs in acidic media. This can be attributed to the escalated degradation of polymer in the acidic environment. On the premises of these facts it can be said that the fabricated PLGA NPs represents a class of sustained release therapeutic vessels which can be used for the effective remediation of varied diseases. Further, the values of correlation coefficient (r^2) obtained after kinetic modeling of in vitro release data suggested a Weibull model. It became imperative from the kinetic modeling that the fabricated BITC-PLGA NPs possessed a matrix type geometry (Table 1).

Stability study

DLS analysis was performed to decipher the intricate stability of BITC-PLGA NPs. Periodic assessment of particle size, and zeta potential was carried out at designated time interval to decipher any change in the initial values of the aforesaid parameters at 4 °C. No apparent change (i.e. aggregation and coalescence) was observed in the physical state of the nanoparticles. Nearly similar particle size and zeta potential values were obtained after a stipulated time period of 30 days (Fig. 2a).

Hemolysis study

To attain an effective therapeutic efficacy, biocompatibility of the fabricated nanosystems becomes mandatory. Hence, hemolysis study was performed to ascertain the safety and efficacy of the formulated nanostructured systems. In the present research endeavors were made to comparatively evaluate the hemo-toxicity of all the test (BITC-PLGA NPs), and control samples (Triton X 100, BITC, PLGA NPs). It can be seen from Fig. 2b among all the samples BITC-PLGA NPs, and pristine PLGA NPs showed minimal toxicity. Whereas, on the other hand, Triton X 100, and BITC in its native state was found to be slightly toxic. This further vouched the desired goal of the current research.

Antibacterial activity

Agar well diffusion assay

The present research primarily focused at evincing an effective strategy to curb the overgrowing menace of bacterial pathogenesis. Hence, a comparative study was performed amidst the test and control samples to streamline the antibacterial efficacy of formulated nanostructured systems against *E. coli*. Herein, agar well diffusion assay was performed,

Table 1 Mathematical modeling of in vitro drug release from BITC-PLGA NPs

Kinetic drug release model (R^2)								
	Zero	First	Second	Third	Higuchi	Weibull	Hickson-Crowell	Korsmeyer-Peppas
pH 5.5	0.6506	0.0594	0.0296	0.0296	0.5237	0.9246	0.3584	0.9133
pH 7.4	0.6648	0.4215	0.2165	0.1092	− 4.6324	0.9801	0.5002	0.9448

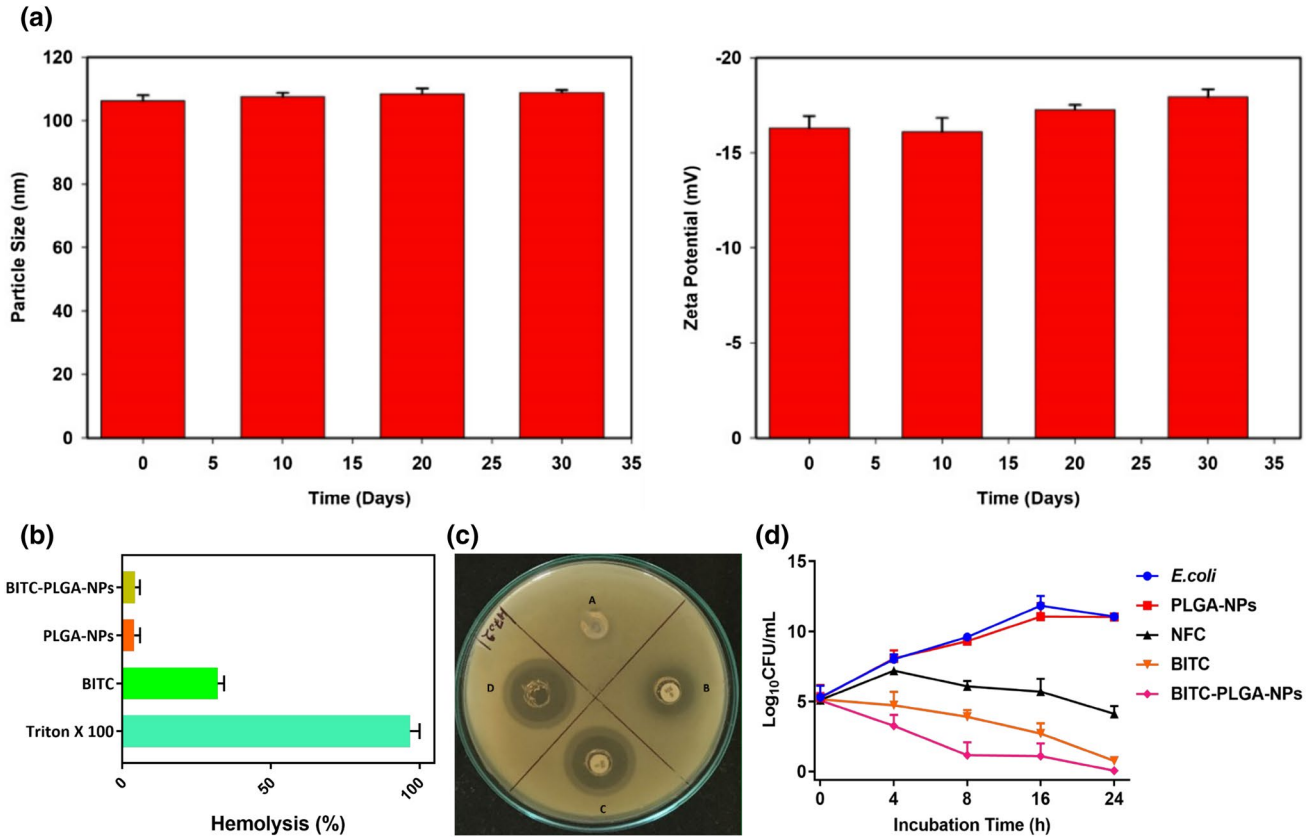

Fig. 2 **a** Long term stability study of BITC-PLGA NPs. **b** Haemolysis study of test and control samples. **c** Antibacterial activity of PLGA NPs, NFC, BITC, BITC-PLGA NPs. **d** Antibacterial kinetics of test formulations against *E. coli*

Table 2 Zone of inhibition developed by varied test samples against bacterial strains

Coding	Antibacterial agents	Zone of inhibition (mm)
A	PLGA-NPs	ND
B	NFC	4
C	BITC	12
D	BITC-PLGA-NPs	14

ND not determined

and the antibacterial efficacy was deciphered in terms of zone of inhibition. Figure 2c and Table 2 documents the outcome of diffusion assay. It can be seen from the figure that, PLGA encapsulated BITC possessed superior bactericidal activity and was found to be highly susceptible against *E. coli* as compared to pristine BITC, NFC and PLGA NPs. The order of magnitude was found to be BITC-PLGA NPs > BITC > NFC > PLGA NPs. The zone of inhibition produced by BITC-PLGA-NPs was found to be 3.5, and 1.16 times larger than the one produced by NFC, and BITC, respectively. It also became evident from the outcome of the study that PLGA-NPs alone could not incite any bactericidal effect, and was found to be bacteriostatic.

These results vouched the main perspective of the present research, and proved that the fabricated nanosystems are capable of generating a synergistic effect against model bacterial strain. This synergism can be predominantly ascribed to the cessation of cell wall synthesis or alteration in the permeability of the cell membrane. However, the exact underlying mechanism behind this enhanced antibacterial activity is yet to be elucidated.

Time kill assay

Quantitative estimation of antibacterial efficacy was assessed via employing a viable cell count methodology. As shown in Fig. 2d, BITC, NFC, and BITC-PLGA NPs have demonstrated an effective antibacterial effect. The order of magnitude was found to be BITC-PLGA NPs > BITC > NFC > PLGA NPs. More interestingly, PLGA NPs encapsulating BITC has shown a prompt, and significant reduction in the colony forming unit (CFU) of *E. coli* as compared to pristine BITC thereby affirming the synergistic effect of the nano-carrier, and the entrapped bioactive compound.

Impact of the study

The present study offers an effective and safe alternative for combating the overgrowing menace of bacterial pathogenesis. The hybrid nanoparticulate system fabricated in the present research provided a protective niche to the model compound, i.e. BITC, thereby, escalating its physicochemical and biological attributes. The potential shortcomings such as biocompatibility, stability, toxicity, and diminished bioavailability which tends to hamper the practical applicability of BITC have been comprehensively overcome by the successful encapsulation of BITC within the framework of polymeric PLGA nanoparticles. CCD-based optimization of requisite process parameters leads to the attainment of certain desirable attributes which can further aid in achieving an escalated therapeutic response. Sustained release of BITC from the PLGA NPs can further prove to be handy in acquiring a targeted delivery of therapeutic agent at a desired dose regimen. It became imperative from all the aforementioned properties that the fabricated BITC-PLGA NPs can lead to an enhanced therapeutic efficacy and better patient compliance. Outcome of the hemocompatibility and antibacterial assay showed that the fabricated nanostructured system can be used as a viable vector for antibacterial treatment in both in vitro and in vivo systems. Morphology and surface property are some of the other imperative factors which tend to govern the ultimate fate of NPs in the designated target site. Herein, the contemplated nanostructured system possessed a uniform and smooth geometry which allowed the NPs to establish an effective bridging with the bacterial cell wall. Infinitesimally small size (nano-size) of these particles also allowed them to smoothly traverse through the cell periphery into the deeper cellular interstitium. Additionally, the surfactant (Vitamin E TPGS) utilized in the formulation is a permeation enhancer, owing to which an enhanced permeation retention (EPR) effect was observed which further escalated the bactericidal potency of the fabricated BITC-PLGA NPs (Wang et al. 2017). Hence, on the premises of these facts and findings, it can be proclaimed that the present nanoparticulate system offers a novel approach to combat bacterial infractions. The present system can also be scaled up in pharmaceutical set up so that the health care sector can immensely benefit from it.

Conclusions

The present work endeavors the innate potential of quasi-solvent emulsification-diffusion method to fabricate BITC-PLGA NPs which will serve as an alternative strategy for enhanced antibacterial remediation. The facile implication of PLGA as a major parent excipient in the fabrication procedure leads to the attainment of several desired attributes such as biocompatibility, enhanced retention time, engineered release characteristics and pristine targeting ability. Whereas, on the other hand, implementation of CCD lead to a systematic optimization of the CMAs thus, aided in achieving the desired CQAs, i.e. minimized size, maximum entrapment efficiency and sustained release profile.

The fabricated BITC-PLGA NPs were nanosized (106.2 ± 1.78 nm) and possessed a homogenous population having narrow size distribution (PDI = 0.353 ± 0.008). The BITC-PLGA NPs depicted highly stabilized nature, as they possessed a significantly high zeta potential value of -16.3 ± 0.64 mV. Long-term stability studies further strengthened this point as the particle size and zeta potential values were found to be nearly identical after a storage period of 30 days. UV–Vis spectroscopy revealed an absorption maxima at 254 nm which is characteristic for BITC. However, the UV–Vis spectra of BITC-PLGA NPs lacked this peak. ATR-FTIR spectra also depicted similar results and the characteristic peak corresponding to the isosulfocyanic group (N=C=S) of BITC was found to be missing in case of BITC-PLGA NPs. These facts and findings pointed towards the facile encapsulation of BITC within the polymeric PLGA matrix.

The lacunas viz. diminished solubility and reduced stability were comprehensively overcome by the fabricated BITC-PLGA NPs. The entrapment efficiency and drug loading of BITC-PLGA NPs was found to be 74 and 32%, respectively. The fabricated BITC-PLGA NPs showed a tri-phasic pattern, and ~ 64.2 (pH 5.5)–83.8 (pH 7.4)% of BITC was released at the end of 168th h. Safety, efficacy and BITC-PLGA NPs was proven by hemolysis profile. Antibacterial assay suggested a synergistic effect and the BITC-PLGA NPs were found to be highly susceptible against *E. coli*. The present study thus offers an excellent polymeric nanoparticulate system with enhanced level of formulation robustness which can be used as a strong antibacterial contingent.

Acknowledgements The authors recognize DST PURSE grant for monetary help. The authors need to extraordinarily offer their thanks towards Dr. Vipasha Sharma and Shikha Kapil (University Institute of Biotechnology, Chandigarh University, Gharuan (Punjab), India) for their consistent help in performing antibacterial activity. We additionally stretch out our vote of gratitude to the SAIF/CIL and CIIPP, Panjab University (Chandigarh), India, for providing FE-SEM, EDS, and DLS facilities, respectively.

Compliance with ethical standards

Conflict of interest The authors reported no potential conflict of interest.

References

Armentano I, Dottori M, Fortunati E, Mattioli S, Kenny J (2010) Biodegradable polymer matrix nanocomposites for tissue engineering: a review polymer degradation and stability 95:2126–2146

Balouiri M, Sadiki M, Ibnsouda SK (2016) Methods for in vitro evaluating antimicrobial activity: a review. J Pharm Anal 6:71–79
Beg S, Saini S, Bandopadhyay S, Katare O, Singh B (2018) QbD-driven development and evaluation of nanostructured lipid carriers (NLCs) of Olmesartan medoxomil employing multivariate statistical techniques. Drug Dev Ind Pharm 44:407–420
Bhujbal SV, de Vos P, Niclou SP (2014) Drug and cell encapsulation: alternative delivery options for the treatment of malignant brain tumors. Adv Drug Deliv Rev 67:142–153
Bohrey S, Chourasiya V, Pandey A (2016) Polymeric nanoparticles containing diazepam: preparation, optimization, characterization, in vitro drug release and release kinetic study. Nano Converg 3:3
Danhier F, Ansorena E, Silva JM, Coco R, Le Breton A, Préat V (2012) PLGA-based nanoparticles: an overview of biomedical applications. J Control Release 161:505–522
Desai K, Park H (2005) Preparation of cross-linked chitosan microspheres by spray drying: effect of cross-linking agent on the properties of spray dried microspheres. J Microencapsul 22:377–395
Dewangan HK, Pandey T, Maurya L, Singh S (2018) Rational design and evaluation of HBsAg polymeric nanoparticles as antigen delivery carriers. Int J Biol Macromol 111:804–812
Dufour V, Stahl M, Baysse C (2015) The antibacterial properties of isothiocyanates. Microbiology 161:229–243
Encinas-Basurto D et al (2017) Poly (lactic-co-glycolic acid) nanoparticles for sustained release of allyl isothiocyanate: characterization, in vitro release and biological activity. J Microencapsul 34:231–242
Fathi M, Mozafari M-R, Mohebbi M (2012) Nanoencapsulation of food ingredients using lipid based delivery systems. Trends Food Sci Technol 23:13–27
Fernandes R, Gracias DH (2012) Self-folding polymeric containers for encapsulation and delivery of drugs. Adv Drug Deliv Rev 64:1579–1589
Francis S, Joseph S, Koshy EP, Mathew B (2018) Microwave assisted green synthesis of silver nanoparticles using leaf extract of elephantopus scaber and its environmental and biological applications. Artif Cells Nanomed Biotechnol 46:795–804
Gaurav P, Yuanyuan S, Juanjuan Z, Xingcai Z, Stefano L (2018) Nanocarriers for targeted delivery and biomedical imaging enhancement. Ther Deliv 9:451–468
Gonzalez-Pizarro R, Silva-Abreu M, Calpena AC, Egea MA, Espina M, García ML (2018) Development of fluorometholone-loaded PLGA nanoparticles for treatment of inflammatory disorders of anterior and posterior segments of the eye. Int J Pharm 547(1–2):338–346
Hanschen FS, Brüggemann N, Brodehl A, Mewis I, Schreiner M, Rohn S, Kroh LW (2012) Characterization of products from the reaction of glucosinolate-derived isothiocyanates with cysteine and lysine derivatives formed in either model systems or broccoli sprouts. J Agric Food Chem 60:7735–7745
Hecht SS (1999) Chemoprevention of cancer by isothiocyanates, modifiers of carcinogen metabolism. J Nutr 129:768S–774S
Ibarra J, Melendres J, Almada M, Burboa MG, Taboada P, Juárez J, Valdez MA (2015) Synthesis and characterization of magnetite/PLGA/chitosan nanoparticles. Mat Res Express 2:095010
Jang SC et al (2013) Bioinspired exosome-mimetic nanovesicles for targeted delivery of chemotherapeutics to malignant tumors. ACS Nano 7:7698–7710
Jiang Z-T, Zhang Q-F, Tian H-L, Li R (2006) The reaction of allyl isothiocyanate with hydroxyl/water and b-cyclodextrin using ultraviolet spectrometry. Food Technol Biotechnol 44:e7
Khoobchandani M, Bansal P, Medhe S, Ganesh N, Srivastava M (2012) Antioxidant and antimutagenic activities of isothiocyanates rich seed oil of Eruca sativa plant. In: Khemani LD, Srivastava MM, Srivastava S (eds) Chemistry of phytopotentials: health, energy and environmental perspectives. Springer, Berlin, Heidelberg, pp 47–51
Kunyi L et al (2018) Construction of functional nanonetwork-structured carbon nitride with Au nanoparticle yolks for highly efficient photocatalytic applications. Chem Comm 54:7159–7162
Li W, Liu X, Yang Q, Zhang N, Du Y, Zhu H (2015) Preparation and characterization of inclusion complex of benzyl isothiocyanate extracted from papaya seed with β-cyclodextrin. Food Chem 184:99–104
Li Y et al (2019) Rational design of silver gradient for studying size effect of silver nanoparticles on contact killing. ACS Biomat Sci Eng 5:425–431
Liu TT, Yang TS (2010) Stability and antimicrobial activity of allyl isothiocyanate during long-term storage in an oil-in-water emulsion. J Food Sci 75:C445–C451
Lü J-M, Wang X, Marin-Muller C, Wang H, Lin PH, Yao Q, Chen C (2009) Current advances in research and clinical applications of PLGA-based nanotechnology. Expert Rev Mol Diagn 9:325–341
Mendyk A, Jachowicz R (2007) Unified methodology of neural analysis in decision support systems built for pharmaceutical technology. Expert Syst Appl 32:1124–1131
Mennicke W, Görler K, Krumbiegel G, Lorenz D, Rittmann N (1988) Studies on the metabolism and excretion of benzyl isothiocyanate in man. Xenobiotica 18:441–447
Ohta Y, Matsui Y, Osawa T, Kawakishi S (2004a) Retarding effects of cyclodextrins on the decomposition of organic isothiocyanates in an aqueous solution. Biosci Biotechnol Biochem 68:671–675
Ohta Y, Takatani K, Kawakishi S (2004b) Effects of ionized cyclodextrin on decomposition of allyl isothiocyanate in alkaline solutions. Biosci Biotechnol Biochem 68:433–435
Prashar A, Siddiqui F, Singh AK (2012) Synthetic and green vegetable isothiocyanates target red blood leukemia cancers. Fitoterapia 83:255–265
Qhattal HSS, Wang S, Salihima T, Srivastava SK, Liu X (2011) Nanoemulsions of cancer chemopreventive agent benzyl isothiocyanate display enhanced solubility, dissolution, and permeability. J Agric Food Chem 59:12396–12404
Rozhkova EA, Ulasov I, Lai B, Dimitrijevic NM, Lesniak MS, Rajh T (2009) A high-performance nanobio photocatalyst for targeted brain cancer therapy. Nano Lett 9:3337–3342
Saka OM, Öz UC, Küçüktürkmen B, Devrim B, Bozkır A (2018) Central composite design for optimization of zoledronic acid loaded PLGA nanoparticles. J Pharm Innov 80:1–12
Sharma S, Parmar A, Kori S, Sandhir R (2016) PLGA-based nanoparticles: a new paradigm in biomedical applications. TrAC Trends Anal Chem 80:30–40
Sharma S, Parmar A, Bhardwaj R, Kaur T (2018) Design and characterization of apocynin loaded PLGA nanoparticles and their in vivo efficacy in hyperoxaluric rats. Curr Drug Deliv 15(7):1020–1027
Shiguo C et al (2019) Insight into multifunctional polyester fabrics finished by one-step ecofriendly strategy. Chem Eng J 358:634–642
Sofrata A, Santangelo EM, Azeem M, Borg-Karlson A-K, Gustafsson A, Pütsep K (2011) Benzyl isothiocyanate, a major component from the roots of Salvadora persica is highly active against Gram-negative bacteria. PLoS One 6:e23045
Wang L, Hu C, Shao L (2017) The antimicrobial activity of nanoparticles: present situation and prospects for the future. Int J Nanomed 12:1227
Wanjing Z et al (2018) Cytocompatible—chitosan based multi-network hydrogels with antimicrobial, cell anti-adhesive and mechanical properties. Carbohydr Polym 202:246–257
Yuan H-N, Yao S-J, Shen L-Q, Mao J-W (2009) Preparation and characterization of inclusion complexes of β-cyclodextrin−BITC and β-cyclodextrin−PEITC. Ind Eng Chem Res 48:5070–5078